atmosphere

MDPI

Article

Numerical Investigation on the PM Emission Potential of Metal Sulphides Open Storage

Maria Grazia Badas *, Valentina Dentoni, Federico Angius and Francesco Pinna

Department of Civil and Environmental Engineering and Architecture (DICAAR), Cagliari University, Via Marengo, 2, 09123 Cagliari, Italy
* Correspondence: mgbadas@unica.it

Abstract: Numerical simulations of the wind flow around isolated stockpiles of bulk material are performed to assess the emission potential (P) of particulate matter (PM) from the pile surfaces exposed to wind erosion (i.e., industrial wind erosion). The analysis is focused on two metal sulphides (lead and zinc sulphides), which are typically stored in the open yards of industrial plants that operate in the commodity sector for the production of non-ferrous metals. The EPA methodology is applied to the numerical simulated flow fields to quantify the effect of the wind stress over the erodible surfaces of the two ores. Two alternative open bay geometries and different volumes of material stocked within the enclosing walls are considered. Moreover, the protective effect of the walls is assessed by comparing the same pile configurations without walls. This is found to be highly dependent on the wind direction, as well as to the pile configuration. A methodology that can be easily customized to specific industrial sites is proposed to define the best storage configuration for PM emission prevention and control.

Keywords: PM emission; industrial wind erosion; computational fluid mechanics; RANS; stockpiles of granular materials; emission prevention and control; air pollution

Citation: Badas, M.G.; Dentoni, V.; Angius, F.; Pinna, F. Numerical Investigation on the PM Emission Potential of Metal Sulphides Open Storage. *Atmosphere* **2022**, *13*, 1417. https://doi.org/10.3390/atmos13091417

Academic Editors: Hui Wang, Zhi Chen, Shuming Ma and Zunaira Asif

Received: 14 July 2022
Accepted: 8 August 2022
Published: 2 September 2022

1. Introduction

When dealing with the environmental impact issues related to the emission of air pollutants from industrial activities (production of energy, production and processing of minerals, metals production, etc.), a number of fugitive dust sources must be taken into consideration, in addition to typical conveyed sources. In fact, those industrial plants often comprise outdoor facilities where the handling, transportation, and storage of bulk materials take place. Depending on the mineralogical and physical properties of the materials involved in the process (raw materials, semi-products, end-products and waste materials), some concerns may arise about the emission of Particle Matter (PM) and the consequent impact on the atmosphere. In fact, fine (d < 10 μm) and ultra-fine fractions (d < 4 μm) of PM might be embodied in the granular material under consideration and released into the air to be transported at long distances from the emission source.

Although it is relatively easy to estimate the Emission Factors (EFs) of conveyed sources, the characterization of fugitive dust sources is rather complicated in relation to the many variables on which the emission phenomenon depends: physical properties of the bulk materials involved in the production processes, transportation cycle and type of earth-moving machinery in use, state of unpaved roads and storage practices, as well as the meteorological conditions of the specific site under consideration.

The availability of consistent site-specific algorithms to be used as input parameters in the prediction of PM dispersion into the air represents, in fact, an essential issue in the Environmental Impact Assessment studies (EIA Directive [1]), which commonly require the implementation of air dispersion codes to estimate the impact at the receptors and validate the effectiveness of risk reduction measures [2,3]. The accuracy of the environmental impact

evaluation (i.e., air dispersion simulation) strongly depends on the consistency of the EFs representing the fugitive dust sources under investigation.

This article specifically deals with the emission of PM from the open storage of solid bulk materials exposed to wind erosion (i.e., industrial wind erosion).

Apart from the typical anemological conditions of the site under consideration, a number of physical variables affect a stockpile emission potential, such as the pile's dimension, shape and orientation, the size distribution of the elementary particles or particles aggregates (PSD or ASD respectively) that form the granular material, and its silt and moisture content. According to the United States Environmental Protection Agency (US-EPA) [4], a substantial difference occurs between stockpiles with limited and unlimited erosion potential. Stockpiles of nonhomogeneous material with non-erodible elements (i.e., particles or particles aggregates larger than 1 cm) have limited erosion potential: when the wind speed exceeds the characteristic threshold friction velocity of the erodible particles/particle aggregates, the pile surfaces are rapidly deprived of their erosion potential until a mechanical disturbance occurs and new erodible elements emerge to be removed by the succeeding erosion event. Stockpiles of homogeneous fine material, on the other hand, may provide a continuous flow of dust aerosol, unless natural or artificially induced crusting binds the erodible grains together. Typical examples of unlimited dust sources are the wide and flat surfaces of the tailing basins (i.e., deposits of metallurgical processing residue) [5,6].

This research deals with the emission of dust from the surfaces of nonhomogeneous material (i.e., limited erosion potential) stacked up against three walls (i.e., open bay storage), which is a storage configuration commonly adopted to prevent raw material contamination (i.e., preserve product requirements) and, at the same time, enables the loading/dumping operations by means of earth-moving vehicles [7].

The simplest and most widely used model to estimate the emission of PM from the open storages of bulk material was developed by the US-EPA [4]. The EPA model (Emission Factor for industrial wind erosion) is based on the results of experimental tests and provides an estimate of the emission potential (P), which depends on the wind field near the pile surfaces. However, only two simple configurations are analyzed by EPA, a flat-top oval stockpile and a conical stockpile. Hence, in order to apply the EPA procedure to different and more complex geometries, the wind field around the stockpile needs to be derived. The pioneering work by Badr and Harion [8] shows how this objective can be pursued by means of numerical simulations. Despite the limitations of this procedure, the feasibility to apply a CFD approach combined with the EPA methodology is meaningful since in operative contexts it would be unfeasible, yet more accurate, to physically test real configurations. A considerable number of recent studies have applied the CFD approach to investigate the effect on the emission of different features in the stockpile set-up. Various stockpile properties and layouts have been analyzed: the impact of pile height for oblong sharp-crested stockpiles [8], the differences in the emission potential of sharp-crested and flat-top heap [9], as well as the emission properties of semi-circular shaped heaps [10].

In particular, the combined implementation of the CFD approach and the EPA methodology has been applied to evaluate the effectiveness of mitigation measures for erosion prevention and control: Santiago et al. [10] investigated the reduction in the emission potential provided by straight and curved windbreak fences, and Cong et al. [11] tested the sheltering effect of multiple stockpiles configurations. Some authors have analyzed the protective effect of porous barriers [12–15], whereas the effect of the open bay walls on the emission potential has not yet been addressed. Numerical simulations and the EPA emission model (Emission Factor for Industrial wind erosion [4]) are hereby applied to quantify the erosion potential of open bay storage of metal sulphides. Different open bay geometries and variable volumes of bulk material are taken into account. The results show a great variability in the erosion potential depending on the wind direction. The outcomes of the simulations were also analyzed to define a methodology to be easily customized to specific industrial sites, aiming at defining the best storage configuration for PM emis-

sion prevention and control, as well as operative protocols to selectively apply traditional protective measures, such as surface watering and particles binding treatments.

2. Materials and Methods

The research study hereby discussed includes some preliminary activities that were mainly focused on the acquisition of relevant information about the case study: the characterization of the two ores under investigation (lead and zinc sulphides) and the definition of the typical and more representative stockpile geometries. As regards the bulk materials, in particular, laboratory tests were performed to derive all physical parameters affecting the erosion/emission phenomenon. Representative samples of lead and zinc sulphides were provided by a major industrial company that operates in the commodity sector for the production of non-ferrous metals. Many details about the materials under investigation and the typical stockpiles configurations were directly acquired by means of field surveys.

The succeeding fundamental phase of the research activity includes the numerical simulation, which was first performed on the EPA reference case (oval flat-topped pile) and then with the 4 realistic open storage configurations.

2.1. EPA Methodology

According to USEPA [4] (AP42—Compilation of air pollutant emission factors-13.2.5 Industrial wind erosion), the particle flow from a dry surface with limited erosion potential (i.e., finite availability of erodible material) can be estimated by means of Equation (1):

$$EF = k \sum_{i=1}^{n} P_i \quad (1)$$

where *EF* (Emission Factor) is expressed in terms of mass emitted by surface unit per year [g/m^{2}yr], k is the particle size multiplier (PM30; PM15; PM10 and PM2.5), *N* is the number of mechanical disturbances per year, which restore the surface emission potential, and *P* is the emission potential corresponding to the observed (or probable) wind fastest mile in the *i*-th period between succeeding mechanical disturbances. The emission potential *P* is expressed in terms of dust emitted per surface unit [g/m^2] by Equation (2):

$$P = 58(u^* - u_t^*)^2 + 25(u^* - u_t^*) \quad (2)$$

where u^* is the friction velocity and u_t^* is the threshold friction velocity of the bulk material under investigation, which is calculated by means of Equation (3):

$$u^* = 0.1 u_s \quad (3)$$

The use of Equation (2) requires the knowledge of the normalized wind speed contours, expressed as the ratio of the average speed at 25 cm (u_s) from the exposed heap surfaces to the average speed of the wind at 10 m (u_r). For two ordinary pile shapes (conical and oval with flat top, with 37° of side slope), EPA provides the required wind contours and thus, the possibility of estimating the overall PM emission over a year time.

2.2. Numerical Simulations

Numerical simulations were performed to solve the flow around different pile configurations and subsequently apply the EPA method. Specifically, the three-dimensional Reynolds Averaged Navier–Stokes (RANS) equations were solved using the open source CFD library OpenFOAM, which has been extensively and successfully used to perform numerical simulations of the wind flow around obstacles both in urban and industrial environments [16–20]. The model numerically solves equations of mass and momentum conservation:

$$\frac{\partial \overline{u}_i}{\partial x_i} = 0 \quad (4)$$

$$\frac{\partial \overline{u}_i}{\partial t} + \frac{\partial \overline{u}_i}{\partial x_j}\overline{u}_j = -\frac{1}{\rho}\frac{\partial \overline{p}}{\partial x_i} - \frac{\partial}{\partial x_j}\left(\nu\frac{\partial \overline{u}_i}{\partial x_j} - \overline{u_i' u_j'}\right), \quad (5)$$

where $\overline{u}_i$ is the mean velocity component along the i direction, $\overline{p}$ is the average pressure, ρ is the density, and ν is the kinematic viscosity of the airflow. In order to model the turbulent Reynolds stresses, $\overline{u_i' u_j'}$, the two-equations k-ε closure is adopted. SimpleFoam, a steady state solver for incompressible turbulent flow, based on the SIMPLE algorithm, is applied. Second order schemes for discretization are adopted, and a threshold of 10^{-6} for scaled residuals is chosen as a convergence criterion [8].

Before applying the numerical model to compute the flow around the configurations of interest (as described in Section 3.2), the model was validated in one of the two simple case studies experimentally investigated by EPA [4]: an oval flat topped pile (coded B1).

Specifically, each of the tested configurations is considered as isolated inside a domain whose dimensions are set according to the literature prescriptions [21], which are aimed at avoiding unwanted acceleration over and around the obstacle. Namely, a directional blockage ratio not exceeding 17% is set in both vertical and horizontal directions. The inlet is 5 H_{max} upstream the obstacle (H_{max} is the pile height), and the outlet is placed 15 H_{max} downstream the pile to allow for the correct wake development. The domain height is 6 H_{max} (Figure 1).

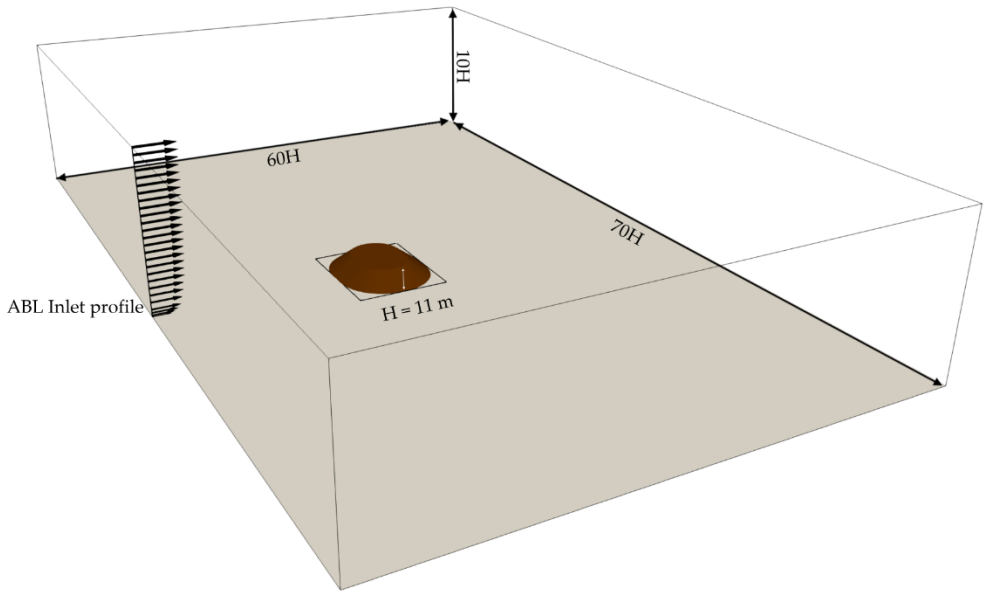

Figure 1. Computational domain used for the simulation of the airflow around EPA oval flat topped pile (coded B1).

As for boundary conditions, an atmospheric logarithmic profile is imposed at the inlet (corresponding to a velocity equal to 13.7 m/s at 10 m in height), a zero-gradient condition at the outlet, and no-slip condition at the walls and on the pile. The near-wall region of the turbulent boundary layer is fully modelled via the use of wall-functions and not resolved explicitly due to the high Reynolds number of the flow, in order to relax the mesh resolution requirement at the wall and reduce the computational effort requested by the model. SnappyHexMesh was used to obtain a body conformal hex-dominant mesh, with local surface and volume refinements (Figure 2). A grid sensitivity test was performed to assess the robustness of the model. For the validation configuration, the adopted computational grids ranged from 0.8 to 3.8 million of cells.

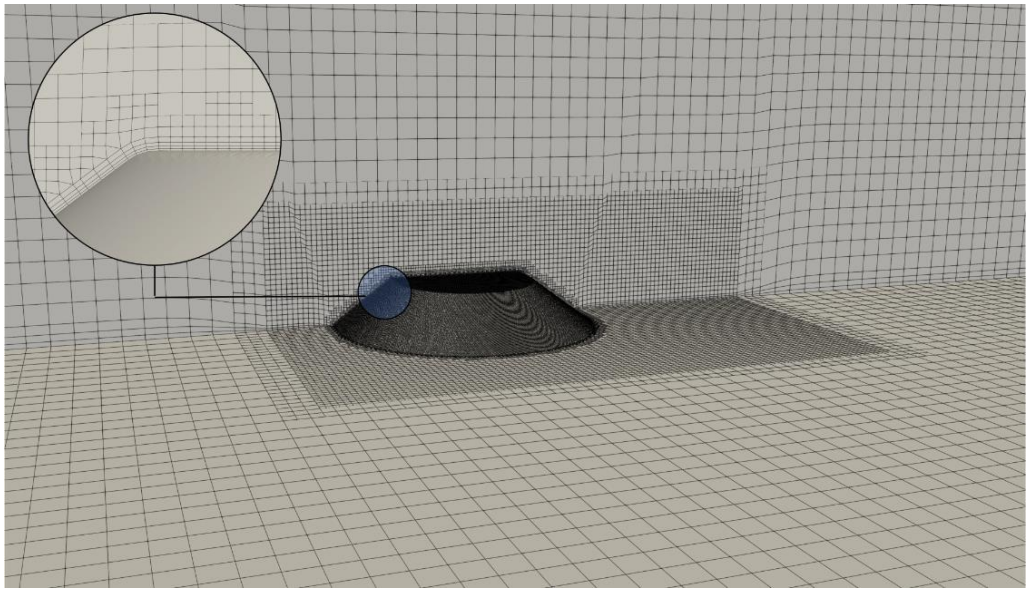

Figure 2. Computational grid for the validation case.

The CFD results, which are not reported here for the sake of brevity, were compared with the EPA experimental results in terms of qualitative airflow, wind exposure, and emission potential. The numerical computation provides a good representation of the flow around the pile and, albeit some inevitable differences in the isosurface of the u_s/u_r ratios, the simulation provides comparable results in terms of emission potential, P, with an overestimation of P lower than 10%. This result is comparable to other numerical studies [10,11].

Hence, despite the inherent limitations of the numerical approach (discussed in Section 4), the model can be considered reliable to assess the airflow around stockpiles and subsequently apply the EPA algorithms to estimate the emission potential (P). Accordingly, the numerical setup adopted for the validation case was applied to the case-studies under investigation (i.e., open bay storages).

2.3. Case Study: Material Characterization

Lead glance (PbS) and zinc blende (ZnS) are two metal sulphides used as raw materials for the production and processing of lead and zinc. The main physical properties of the two materials under investigation were derived from representative samples of 30 × 30 cm, deprived of their coarser fraction (particle aggregates with diameter larger than 1 cm), and oven-dried for 48 h at 40 °C up to a 3% residual moisture content (assumed as dry condition). A nest of sieves with openings of 4, 2, 1, 0.5, and 0.25 mm was used to perform the aggregate size analysis, according to the procedure suggested by EPA [4]. The histogram in Figure 3 represents the mean aggregate size distribution (ASD) for the two ores. The results of the ASD analysis show that the lead glance contains a higher percentage of small aggregates (i.e., lower mode) compared to the zinc blend: this outcome can be explained by the greater cohesion energy of the zinc blende elementary particles [22]. Table 1 reports the relative quantities of catch within each sieve, the ASD mode, and the inferred threshold friction velocity (u_t^*) [4,23], and shows that lower values of u_t^* are associated to the lead glance, with a resulting u_t^* (PbS)/u_t^* (ZnS) ratio of 0.72.

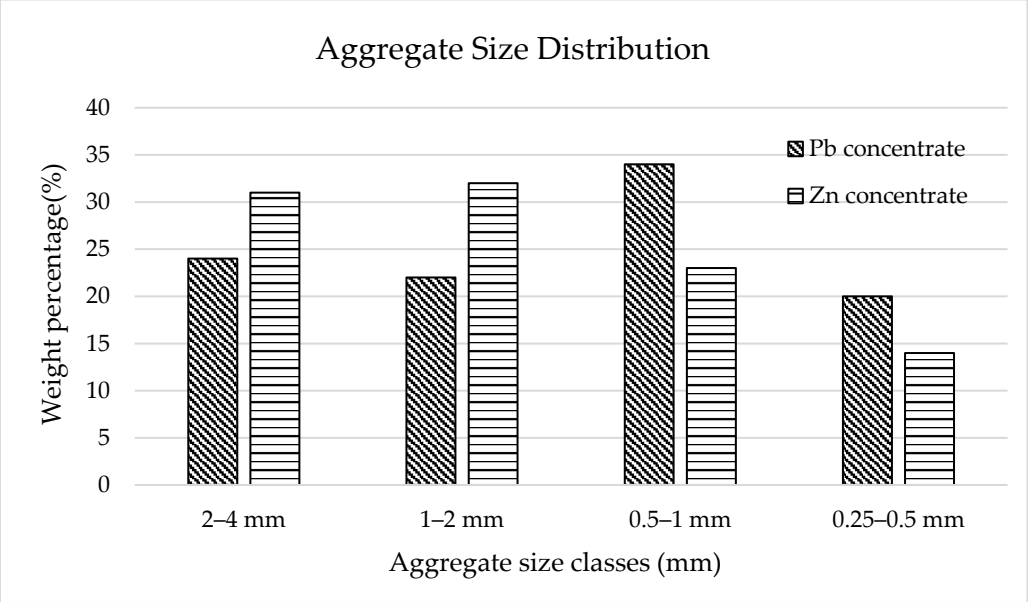

Figure 3. Aggregate size distribution for the samples of Lead and Zinc sulphides.

Table 1. Aggregate size distribution and derived threshold friction velocity [4].

		Opening Size (mm)				Mode	u_t^*
Material	**Moisture Content**	**2 < d < 4**	**1 < d < 2**	**0.5 < d < 1**	**0.25 < d < 0.5**	**mm**	**m/s**
Lead Glance	2.5%	24%	22%	34%	20%	0.75	0.58
Zinc Blende	2.5%	31%	32%	23%	14%	1.50	0.76

In addition to the ASD analysis, PM emission tests were carried out in the Environmental Wind Tunnel (EWT) recently designed and set up in the laboratories of Cagliari University: PM concentration values were measured at 2.0 cm from the ore samples for increasing wind velocity, by means of an optical analyzer (DUSTTRAK DRX 8533). Table 2 reports the mean values of the threshold velocity at 2.0 cm ($ut_{2.0}$) for the two materials under investigation and the corresponding values at 25 cm (ut_{25}), which were derived from the wind profiles simulated in the tunnel [6]. The ratio u_t (PbS)/u_t (ZnS) obtained from the tunnel tests is roughly 0.76, and thus in agreement with the ratio u_t^* (PbS)/u_t^* (ZnS) derived from the ASD analysis (Table 1).

Table 2. Key properties of lead and zinc sulphides.

Material	**Dispersiveness Class**	**Density (g/cm^3)**	**Threshold Velocity $ut_{2.0}$ (m/s)**	**Threshold Velocity ut_{25} (m/s)**
Lead glance	S2	7.6	4.38	6.5
Zinc blende	S4	4.0	6.11	8.5

Table 2 also reports the density of the two materials (from the technical data sheets) and the dispersiveness class reported by the IPPC Reference document (Integrated Pollution Prevention and Control) [7], in accordance to the classification suggested by Netherland Emission Guidelines for air [24], which indicates a higher dispersion hazard for the lead glance (S2—highly drift sensitive) compared to the zinc blende (S4—moderately drift sensitive). The higher emission potential of the lead glance is also confirmed by the results of a recent study on the effect of the material physical properties on the erosion/emission mechanisms [22].

2.4. Case Study: Stockpiles Configurations

According to the IPPC Reference document [7], open bays are defined as heaps enclosed within three walls and are commonly used for storage of ore and concentrates in the production and processing of metals. The four open bay configurations represented in Figure 4 were hereby analyzed (two planar footprints and two pile heights): a high rectangular pile (HR, plot a), a low rectangular pile (LR, plot b), a high square pile (HS, plot c), and a low square pile (LS, plot d).

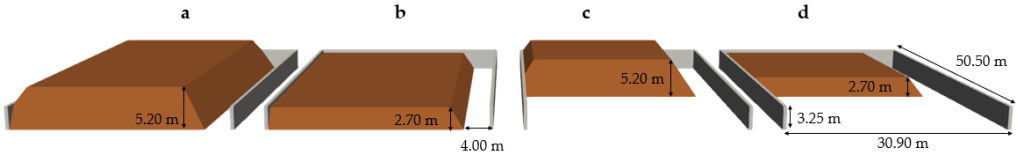

Figure 4. Sketch of the heap and analyzed configurations: high rectangular pile (HR, plot **a**), low rectangular pile (LR, plot **b**), high square pile (HS, plot **c**), and low square pile (LS, plot **d**).

The adopted configurations allow for the understanding of the effectiveness of the enclosing walls in different operative conditions: fully (a and b plots) and partially filled (c and d plots) bays and height of stacked material exceeding (a and c cases, H_{max} = 5.20 m), or not (b and d cases, H_{max} = 2.70 m), the bay walls (H = 3.00 m). The numerical simulations were performed with and without U-shape enclosing walls, while the open bay was rotated inside the domain to consider 24 incoming wind directions. The variation of the wind direction allows in fact a comprehensive analysis of the wall effectiveness under different exposure conditions. This may be useful to assess the best stockpile orientation with respect to the prevailing winds or, if coupled to a wind rose of a specific site, to assess the overall potential erosion risk according to the local meteorological conditions.

In order to simulate the flow field inside a fixed domain (i.e., fixed dimension for all the cases under investigation) and, at the same time, maintain the blockage ratio adopted for the validation case, the size of the numerical domain was defined on the basis of the diagonal dimension (L_{max} = 59.2 m ≈ 60 m) and the maximum height (H_{max} = 5.2 m ≈ 6 m) of the heap. As shown in Figure 5, the conservativeness of the condition on the directional blockage ratio determines a wider domain in the spanwise than in the streamwise direction.

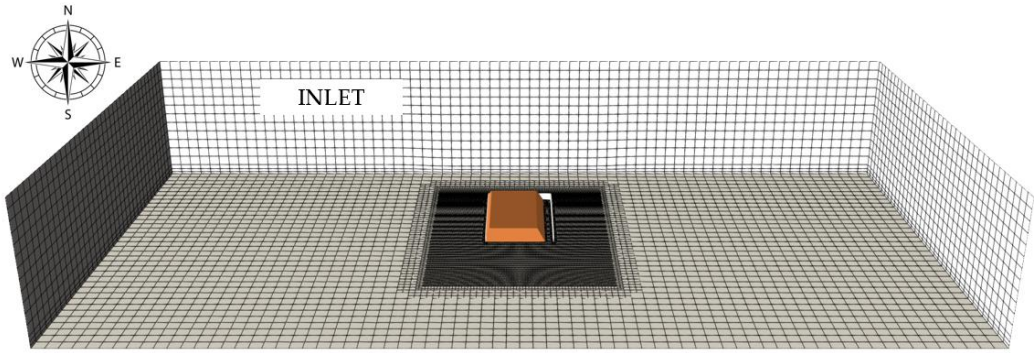

Figure 5. Computational domain and numerical grid. Example for HR configuration and wind coming from North.

An incoming logarithmic profile was simulated, with U_{ref} = 13.5 m/s at z_{ref} = 10 m (i.e., U_{10}) and roughness height z_0 = 0.5 m on the bottom, which corresponds to rough terrain (i.e., industrial settlements), according to the Davenport-Wieringa classification [25]. This profile corresponds to turbulent conditions, with a Reynolds number (based on the inlet velocity at the obstacle height) greater than the critical condition for the flow to be independent of the Reynolds number (i.e., 15,000 [26]). This guarantees the normalized wind speed ratios, u_s/u_r, to be independent of the wind speed of the incoming flow, U_{10}.

3. Results

3.1. Flow Patterns over the Stockpiles

The flow topology around an open bay storage is more complex compared to the case of an isolated pile without confining walls. First of all, the open bay storage does not have any symmetry axis, due to the presence of a corridor along one side of the pile (from the bay entrance to the enclosing transversal wall), where the transit of earth-moving machinery must be allowed to perform loading and unloading operations. Therefore, the flow is asymmetrical regardless of the wind direction.

Figure 6 shows the streamlines around heaps higher than the enclosing walls, for a rectangular planar section (HR, left panel) and a square planar section (HS, right panel), under the assumption of SE incoming wind. It becomes apparent how the airflow enters the corridor to exert its influence on the non-protected side of the pile. In addition to the flow topology, the results of the present study include the u_s/u_r maps (i.e., normalized wind speed contours), with the partition of the pile surface proposed by EPA. Figure 7 shows the u_s/u_r isosurface areas (A, B, C and D) for the two cases in Figure 6. As expected, the simulations proved that both the heap geometry and the wind direction have a great influence on the velocity ratio distribution.

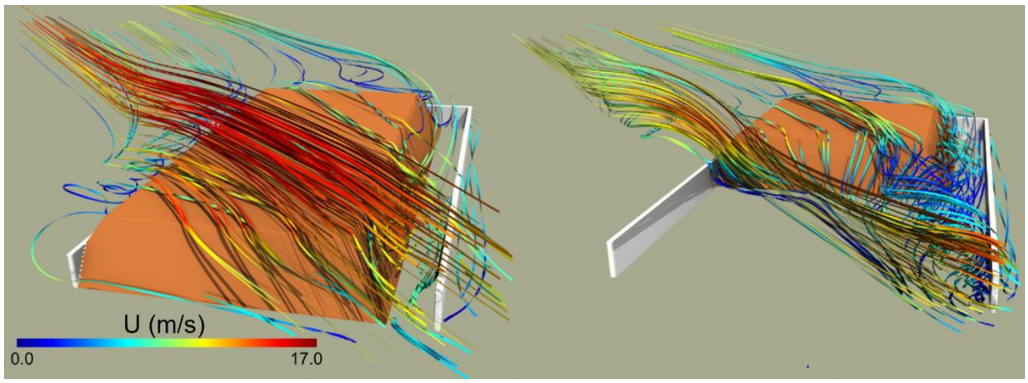

Figure 6. Streamlines over and around a high rectangular heap (HR, **left** plot) and a high square heap (HS, **right** plot) with enclosing walls and SE incoming wind.

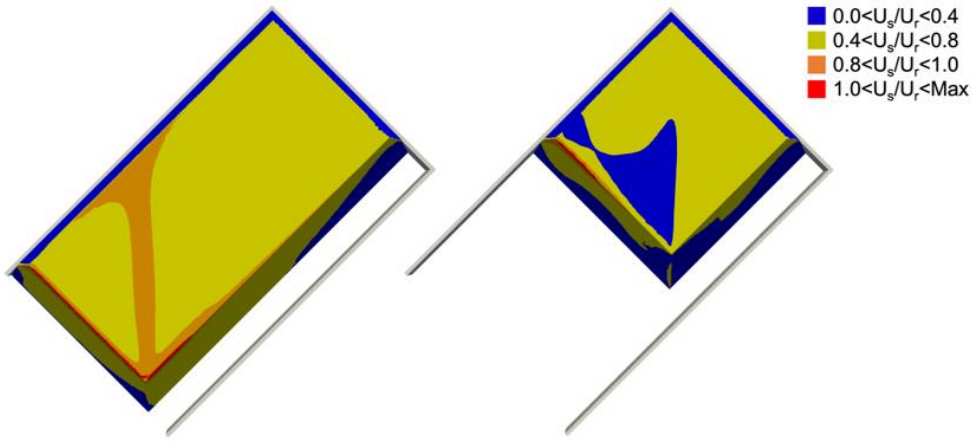

Figure 7. Example of the u_s/u_r isosurface areas according to the EPA classes for the two cases in Figure 6 (HR, **left** plot and HS, **right** plot).

3.2. Impact of Protective Enclosures on Wind Exposure and Emission Potential

The simulations performed for the four open bay configurations were reiterated for the whole set of wind directions considering heaps with same geometry but without enclosing walls, so as to assess their protecting role. Hence, the EPA model (Equations (2) and (3)) was applied to evaluate the emission potential (P) in the case of an incoming

wind U_{10} = 13.7 m/s. The integrated results over the pile surfaces are portrayed as polar plots in Figure 8, for the Lead Glance (u_t^* =0.58 m/s, Table 1), to enable the comparisons of the two cases (with and without protective walls, respectively blue and red lines): each plot refers to a specific pile geometry (HR, LR, HS, LS).

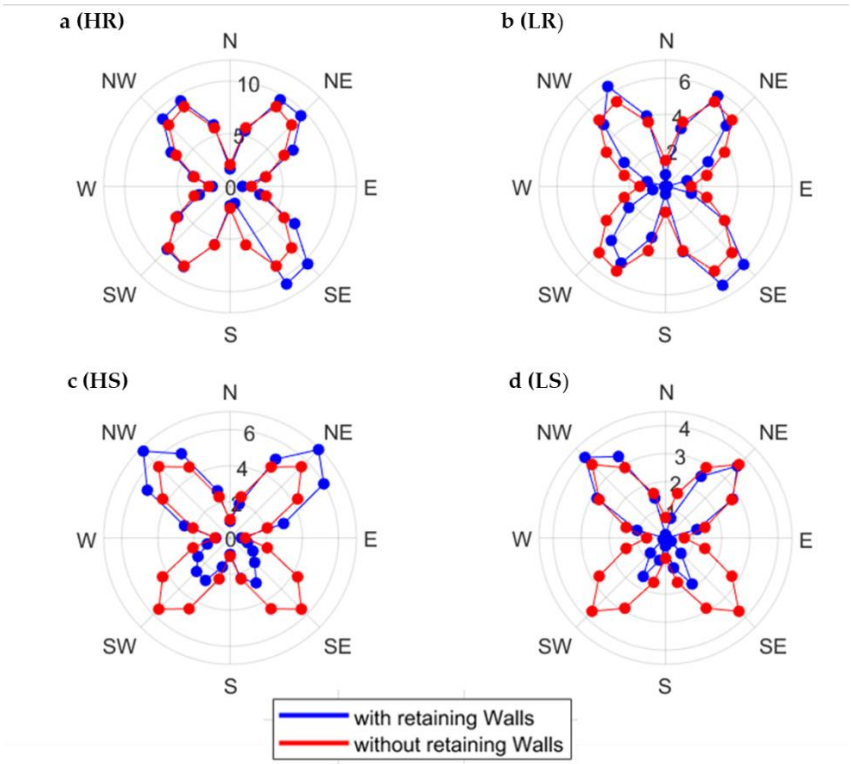

Figure 8. Polar diagram of PM emission potential (P) integrated over the surface of a Lead Glance stockpile for different geometrical configurations ((**a**)HR, (**b**) LR, (**c**) HS, and (**d**) LS). Blue and red lines refer to the configurations with and without enclosing walls.

The application of the EPA model to the wind flow simulation around the heaps gives a clear indication of the enclosing walls effectiveness, as well as on the influence of the heap volume and orientation. Simulations around an isolate pile without enclosing walls obviously provide symmetric results with respect to both the longitudinal and transversal axes (namely N-S and E-W directions). The maximum emission values are attained along the diagonal directions, whereas the emission dramatically drops when the wind is aligned with the pile axes. Since the polar plots in Figure 8 represent the emission potential (P) given by the integrational contribution of each emitting sub-area (defined by the wind speed contours), for a given approaching wind, its maximum value decreases with decreasing exposed surfaces (i.e., decreasing pile planar projection or decreasing pile heigh).

The outcomes displayed in Figure 8 for a Lead Glance stockpile can be summarized as follows:

- the wind direction has a prominent role and produces lower P values for all the analyzed conditions when it is aligned along the heap main axes;
- when the incident wind is oblique, it produces flow separation on the heap, which leads to higher P values;
- square stockpiles (plot c and d in Figure 8) are very well protected from the enclosing walls when the wind comes from the southern directions (SW-S-SE), corresponding to the open bay entrance. Indeed, the lower *wings* of the butterfly diagram are much smaller than in the case without retaining walls. On the contrary, when the wind comes from the northern quadrants (NW-N-NE), hence from the back of the heap, this beneficial effect is negligible or more often detrimental; and

- rectangular stockpiles (plots a and b of Figure 8) present quite similar P values to the corresponding stockpiles without enclosure. It becomes apparent how SE winds that enter the corridor inside the bay determine, as already observed (Figure 6), recirculation zones and finally an increase in the resulting P.

3.3. Operative Evaluaton of Wind Exposure

When applying the EPA methodology, only the sub-surfaces where the shear velocity exceeds the threshold value (velocity value that triggers the erosion) contribute to the overall PM emission. Hence, in order to operatively use the dataset obtained with the numerical simulations, the Empirical Cumulative Distribution Function (ECDF) of the u_s/u_r ratio can be used.

As an example, Figure 9 shows the ECDF corresponding to one of the 24 wind directions for the low rectangular heap (LR). For each dimensional value U_{10} (i.e., value of the reference velocity u_r at 10 m) reported in the top two axes (one for each of the two materials), the intercept with the ECDF function indicates the percentage of the pile surface that does not contribute to dust emission (% of non-emitting surface), as for that value (U_{10}), the wind velocity near the pile surface ($u_s = u_{25}$) is below the characteristic threshold value of the material under consideration (u_{t25}): 6.5 m/s for Lead Glance and 8.5 m/s for the Zinc Blend (Table 2).

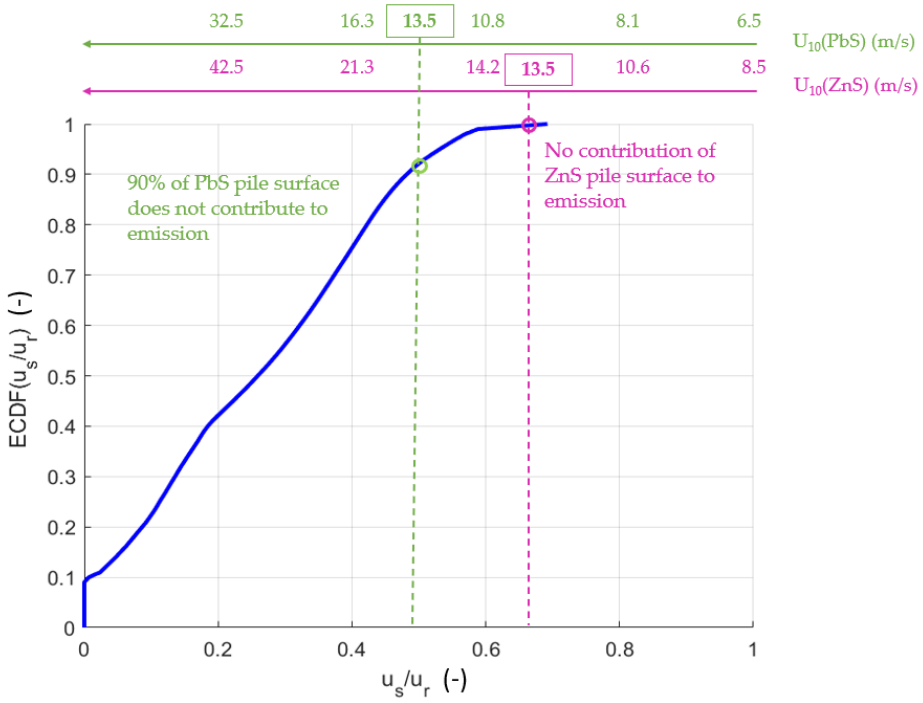

Figure 9. Empirical cumulative distribution function of u_s/u_r ratio for a low rectangular heap (LR) and wind from North. Lead Glance (green, PbS); and Zinc Blende (magenta, ZnS).

In the example of Figure 9, for the incoming wind velocity U_{10} = 13.5 m/s, 90% of the Lead Glance heap is protected by wind erosion, whereas almost all the Zinc Blende heap does not emit. Obviously, higher portions of the pile surface are prone to PM emission for increasing U_{10}, since the threshold value u_{t25} is reached in wider areas.

The implementation of the ECDF function for a given bulk material might represent a useful operative tool to preliminarily assess the emission potential of a stockpile and plan when and where to activate mitigation measures.

Figure 10 shows the ECDF envelopes obtained for a high-square heap (HS) of Lead Glance (PbS), with and without an enclosing wall, for a given wind direction (around 135° ± 15°). The black dashed lines indicate incoming wind velocity U_{10} in the range 10–15 m/s: these

conditions determine a range of non-emitting surfaces between 65–97% in the presence of enclosing walls and between 35–75% for a heap without protection.

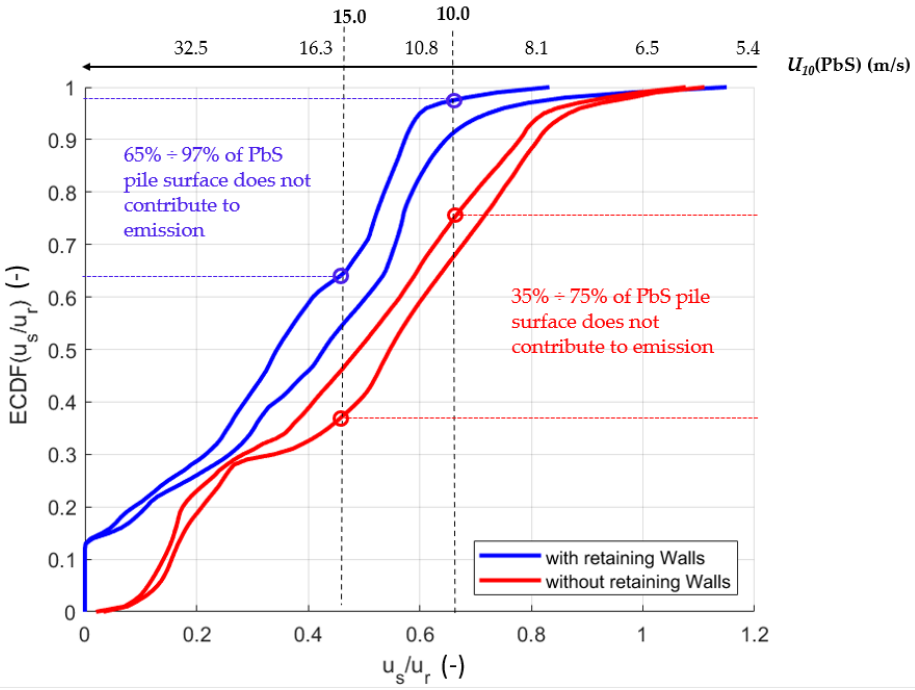

Figure 10. Envelopes of empirical cumulative distribution function of u_s/u_r ratio for a high-square Lead Glance stockpile, with and without enclosing walls (respectively blue and red lines), for incoming SE wind (135° ± 15°).

In general, the wider the ECDF envelope for a given operative condition (with or without enclosing walls), the more scattered the results for different wind directions. The protective effect of the walls in a heap corresponds to the shift of the u_s/u_r ECDF towards the left.

4. Discussion: Limitations and Practical Implications

The study is affected by some inherent limitations. Although friction velocity on the stockpile surface can be directly computed from shear stresses obtained from the simulation, the choice of applying the simplified EPA relationship (Equation (3)) was preferred, since u_s/u_r ratio are less dependent on the simulation setup, and more coherent results with the EPA validation case were obtained when applying the same procedure. Moreover, the presence of other obstacles or buildings, as well as the shadow effect in case of layouts with multiple stockpiles highly affect the flow patterns, exerting a different effect according to the wind direction [9,11]. Nonetheless, the choice of examining isolated stockpiles and modelling the incoming flow over a homogeneous terrain without explicitly considering other nearby obstacles or orographic effects was here motivated by the aim of isolating the sole contribution of the enclosing walls on the reduction of pile fugitive emission.

It is also worthwhile recalling that other factors highly affect the emission, such as the type of material, the moisture content, and the presence of crusts or of film protection. Emissions from operative tasks such material stacking and reclaiming operations, as well as deposition on the yard (around the pile) and re-lifting [27] are not considered, since they are not accounted by the EPA model, although Furieri et al. [28] demonstrated their important contribution to the total emission of an open storage yard.

Even though a more accurate numerical modeling approach, such as Large Eddy Simulations, may be applied, RANS is still considered to be an appropriate computational technique for engineering evaluations [21].

Despite these inherent simplifications, the analysis hereby proposed gives an insight on the effect of heap position and filling on the emission potential, and provides a measure of the protective role of enclosing walls for different wind directions.

Apart from the scientific interest of understanding the complex modification of the flow field depending on the specific operating conditions, and consequent emission potential outcomes, results are important also in view of the need of guidelines and practical methods to assess the effectiveness of structural protection/pile configuration and their integration with temporary measures. Even though the numerical results of this study have to be applied to other configurations with caution, the proposed procedure (including polar plots of emission potential and CDF velocity threshold computation) can also be applied to specific industrial sites. This would require an explicit modelling of the heaps together with the surroundings, as well as the characterization of the solid bulk material under consideration. Results can be used both to optimize the pile orientation with respect to the prevailing winds (also considering the relative location of sensible receptors) and provide useful indications to implement selective mitigation measures. Specifically, the integration of temporary/active protective measures of risk reduction, such as surface moistening and treatment with dust binding substances, could be triggered by the implementation of wind speed monitoring devices, which allow a selective action over specific pile areas when the wind speed threshold is reached.

5. Conclusions

A numerical research was carried out to study the emission potential of isolated stockpiles of bulk material (lead and zinc sulphides) exposed to wind erosion. The EPA method applied to RANS-derived flow fields revealed substantial differences in the emission potential depending on wind directions and open bay configurations. Moreover, the protective effect of the walls was assessed by also performing the numerical simulations on the pile configurations without enclosing walls, and their role was found to be highly dependent both on the wind direction and on the pile setup.

The use of empirical cumulative distribution functions (ECDF) of velocity ratios on the pile surface was proposed to define a methodology to be easily customized to specific industrial sites, aiming at defining the best storage configuration for PM emission prevention and control according to the prevailing winds. The obtained results may also represent a valuable contribution to implement operative protocols to selectively apply traditional protective measures on highly exposed stockpile regions.

Author Contributions: Conceptualization, M.G.B. and V.D.; methodology, M.G.B., V.D., F.A. and F.P.; software, M.G.B. and F.A.; laboratory results, V.D. and F.P.; formal analysis, M.G.B., V.D., F.A. and F.P.; investigation, M.G.B., V.D., F.A. and F.P.; writing—original draft preparation, M.G.B. and V.D.; writing—review and editing, M.G.B. and V.D. All authors have read and agreed to the published version of the manuscript.

Funding: This research was funded by Fondazione Banco di Sardegna, under the research project "RE-MINE-REstoration and remediation of abandoned MINE sites" Fondazione di Sardegna CUP F72F16003160002.

Institutional Review Board Statement: Not applicable.

Informed Consent Statement: Not applicable.

Data Availability Statement: The data that support the findings of this study are available from the corresponding author upon reasonable request.

Conflicts of Interest: The authors declare no conflict of interest.

References

1. Directive 2008/50/EC of the European Parliament and of the Council of 21 May 2008 on Ambient Air Quality and Cleaner Air for Europe. Available online: https://eur-lex.europa.eu/legal-content/EN/TXT/HTML/?uri=CELEX:02008L0050-20150918&from=EN (accessed on 2 August 2022).
2. Piras, L.; Dentoni, V.; Massacci, G.; Lowndes, I.S. Dust Dispersion from Haul Roads in Complex Terrain: The Case of a Mineral Reclamation Site Located in Sardinia (Italy). *Int. J. Min. Reclam. Environ.* **2014**, *28*, 323–341. [CrossRef]
3. Dentoni, V.; Grosso, B.; Pinna, F. Experimental Evaluation of PM Emission from Red Mud Basins Exposed to Wind Erosion. *Minerals* **2021**, *11*, 405. [CrossRef]
4. US EPA, AP-42: Compilation of Air Emissions Factors. Available online: https://www.epa.gov/air-emissions-factors-and-quantification/ap-42-compilation-air-emissions-factors (accessed on 15 June 2022).
5. Dentoni, V.; Grosso, B.; Massacci, G. Environmental Sustainability of the Alumina Industry in Western Europe. *Sustainability* **2014**, *6*, 9477–9493. [CrossRef]
6. Dentoni, V.; Grosso, B.; Massacci, G.; Pinna, F. Validation of a Wind Erosion Model for Tailings Basins: Wind Tunnel Design and Atmospheric Boundary Layer Simulation. *Int. J. Min. Reclam. Environ.* **2020**, *34*, 562–572. [CrossRef]
7. European Commission Emissions from Storage. Integrated Pollution Prevention and Control Reference Document on Best Available Techniques on Emissions from Storage (BAT). 2006. Available online: https://eippcb.jrc.ec.europa.eu/sites/default/files/2022-03/efs_bref_0706_0.pdf (accessed on 15 June 2022).
8. Badr, T.; Harion, J.L. Numerical Modelling of Flow over Stockpiles: Implications on Dust Emissions. *Atmos. Environ.* **2005**, *39*, 5576–5584. [CrossRef]
9. Turpin, C.; Harion, J.-L. Effect of the Topography of an Industrial Site on Dust Emissions from Open Storage Yards. *Environ Fluid Mech.* **2010**, *10*, 677–690. [CrossRef]
10. Toraño, J.A.; Rodriguez, R.; Diego, I.; Rivas, J.M.; Pelegry, A. Influence of the Pile Shape on Wind Erosion CFD Emission Simulation. *Appl. Math. Model.* **2007**, *31*, 2487–2502. [CrossRef]
11. Cong, X.C.; Yang, S.L.; Cao, S.Q.; Chen, Z.L.; Dai, M.X.; Peng, S.T. Effect of Aggregate Stockpile Configuration and Layout on Dust Emissions in an Open Yard. *Appl. Math. Model.* **2012**, *36*, 5482–5491. [CrossRef]
12. Yeh, C.-P.; Tsai, C.-H.; Yang, R.-J. An Investigation into the Sheltering Performance of Porous Windbreaks under Various Wind Directions. *J. Wind Eng. Ind. Aerodyn.* **2010**, *98*, 520–532. [CrossRef]
13. Cong, X.C.; Cao, S.Q.; Chen, Z.L.; Peng, S.T.; Yang, S.L. Impact of the Installation Scenario of Porous Fences on Wind-Blown Particle Emission in Open Coal Yards. *Atmos. Environ.* **2011**, *45*, 5247–5253. [CrossRef]
14. Ferreira, A.D.; Lambert, R.J. Numerical and Wind Tunnel Modeling on the Windbreak Effectiveness to Control the Aeolian Erosion of Conical Stockpiles. *Environ. Fluid Mech.* **2011**, *11*, 61–76. [CrossRef]
15. Song, C.-F.; Peng, L.; Cao, J.-J.; Mu, L.; Bai, H.-L.; Liu, X.-F. Numerical Simulation of Airflow Structure and Dust Emissions behind Porous Fences Used to Shelter Open Storage Piles. *Aerosol Air Qual. Res.* **2014**, *14*, 1584–1592. [CrossRef]
16. Badas, M.G.; Ferrari, S.; Garau, M.; Querzoli, G. On the Effect of Gable Roof on Natural Ventilation in Two-Dimensional Urban Canyons. *J. Wind Eng. Ind. Aerodyn.* **2017**, *162*, 24–34. [CrossRef]
17. Badas, M.G.; Garau, M.; Querzoli, G. How Gable Roofs Change the Mechanisms of Turbulent Vertical Momentum Transfer: A LES Study on Two-Dimensional Urban Canyons. *J. Wind Eng. Ind. Aerodyn.* **2021**, *209*, 104432. [CrossRef]
18. Flores, F.; Garreaud, R.; Muñoz, R.C. OpenFOAM Applied to the CFD Simulation of Turbulent Buoyant Atmospheric Flows and Pollutant Dispersion inside Large Open Pit Mines under Intense Insolation. *Comput. Fluids* **2014**, *90*, 72–87. [CrossRef]
19. Franke, J.; Sturm, M.; Kalmbach, C. Validation of OpenFOAM 1.6.x with the German VDI Guideline for Obstacle Resolving Micro-Scale Models. *J. Wind Eng. Ind. Aerodyn.* **2012**, *104–106*, 350–359. [CrossRef]
20. Joseph, G.M.D.; Lowndes, I.S.; Hargreaves, D.M. A Computational Study of Particulate Emissions from Old Moor Quarry, UK. *J. Wind Eng. Ind. Aerodyn.* **2018**, *172*, 68–84. [CrossRef]
21. Blocken, B. Computational Fluid Dynamics for Urban Physics: Importance, Scales, Possibilities, Limitations and Ten Tips and Tricks towards Accurate and Reliable Simulations. *Build. Environ.* **2015**, *91*, 219–245. [CrossRef]
22. Dentoni, V.; Grosso, B.; Pinna, F.; Lai, A.; Bouarour, O. Emission of Fine Dust from Open Storage of Industrial Materials Exposed to Wind Erosion. *Atmosphere* **2022**, *13*, 320. [CrossRef]
23. Chepil, W.S. Dynamics of wind erosion: II Initiation of soil movement. *Soil Sci.* **1945**, *60*, 397. [CrossRef]
24. Informatiecentrum Milieuvergunningen. *Netherlands Emission Guidelines for Air*; InfoMil: Den Haag, The Netherlands, 2001; ISBN 978-90-76323-03-9.
25. Wieringa, J. Updating the Davenport Roughness Classification. *J. Wind Eng. Ind. Aerodyn.* **1992**, *41*, 357–368. [CrossRef]
26. Snyder, W.H. *Guideline for Fluid Modeling of Atmospheric Diffusion*; Environmental Protection Agency: Washington, DC, USA, 1981.
27. Boente, C.; Millán-Martínez, M.; Sánchez de la Campa, A.M.; Sánchez-Rodas, D.; de la Rosa, J.D. Physicochemical Assessment of Atmospheric Particulate Matter Emissions during Open-Pit Mining Operations in a Massive Sulphide Ore Exploitation. *Atmos. Pollut. Res.* **2022**, *13*, 101391. [CrossRef]
28. Furieri, B.; Santos, J.M.; Russeil, S.; Harion, J.-L. Aeolian Erosion of Storage Piles Yards: Contribution of the Surrounding Areas. *Environ. Fluid Mech.* **2014**, *14*, 51–67. [CrossRef]